Available online at www.sciencedirect.com
ScienceDirect
Journal of Solid State Chemistry 180 (2007) 1198–1208
JOURNAL OF SOLID STATE CHEMISTRY
www.elsevier.com/locate/jssc

Vibrational spectra and H-bondings in anhydrous and monohydrate α-Zr phosphates

Mario Casciola[a], Anna Donnadio[a], Francesca Montanari[a], Paolo Piaggio[b,*], Valeria Valentini[b]

[a]*Dipartimento di Chimica and CEMIN, Centro di Eccellenza Materiali Innovativi Nanostrutturati, Università di Perugia, Via Elce di Sotto, 8. 06123 Perugia, Italy*
[b]*Dipartimento di Chimica e Chimica Industriale, Università di Genova, Via Dodecaneso 31. 16146 Genova, Italy*

Received 30 August 2006; received in revised form 10 January 2007; accepted 12 January 2007
Available online 26 January 2007

Abstract

A new FTIR and FT-Raman investigation on α-zirconium phosphate ($Zr(HPO_4)_2 \cdot H_2O$) and its anhydrous form has been performed in order to obtain an affordable assignment of their vibrational spectra as well as to highlight the hydrogen bonding structure formed by the P-OH groups and the intercalated water molecules. To this end the spectral changes induced by both temperature and isotopic exchange were observed on several high-purity grade samples of different morphology especially prepared and well characterized by SEM, RX, DSC and TGA. In particular, it is also presented as a detailed discussion of the results obtained by FTIR-PAS for different sample morphology. The observed spectra have been analyzed and interpreted according to the α-$Zr(HPO_4)_2 \cdot H_2O$ crystal structure and H-bond geometry. The obtained results allowed to clarify the mechanism of the α-$Zr(HPO_4)_2 \cdot H_2O \rightarrow$ α-$Zr(HPO_4)_2$ dehydration process as well as the H-bonding changes involved in the high temperature phase transition of anhydrous α-$Zr(HPO_4)_2$.

Keywords: Zr phosphates; Vibrational spectra; FTIR-PAS; H-bondings; Phase transitions

1. Introduction

Vibrational spectroscopy, together with diffractometry, calorimetry and electron microscopy, allows studying the chemical structure of a material as well as the modifications induced by physical and chemical processes. In particular, infrared and Raman spectra become a key tool to investigate structures when X-rays are inapplicable like, for instance, in the case of nanosamples.

In the last few years, increasing attention has been focused on the development of polymeric nanocomposites loaded with inorganic materials. Among these, nanoparticles of α-zirconium phosphate (α-$Zr(HPO_4)_2 \cdot H_2O$) were used as fillers of proton-conducting membranes made of Nafion [1–7] and sulfonated polyetherketones [8–13] in order to improve the performance of proton exchange membrane fuel cells in terms of reduction of fuel cross-over and increase of working temperature above 100 °C. More recently, nanosized α- and γ-zirconium phosphates were also used to obtain nanocomposites based on neutral polymers such as epoxy resins [14,15], polyacrylamide [16], polystyrene [17] and polyvinylidenefluoride [18].

α-$Zr(HPO_4)_2 \cdot H_2O$ is a layered ion exchanger [19,20]. Each layer consists of zirconium atoms lying slightly above and below the mean plane and bridged by monohydrogen phosphate groups placed alternatively above and below the plane. Three oxygen atoms of each phosphate group are bonded to three zirconium atoms, while the hydroxyl group points to the interlayer region. The arrangement of adjacent layers creates six-sided cavities. Each cavity accommodates one water molecule forming a network of intra-layer hydrogen bonds with the phosphate hydroxyls. There are no interlayer hydrogen bonds, and only Van der Waals forces hold the layers together [21,22].

*Corresponding author. Fax: +39 10 353873.
E-mail address: piaggio@chimica.unige.it (P. Piaggio).

0022-4596/$ - see front matter © 2007 Elsevier Inc. All rights reserved.
doi:10.1016/j.jssc.2007.01.016

In spite of the great interest in the chemistry of α-$Zr(HPO_4)_2 \cdot H_2O$, the few studies performed by vibrational spectroscopy offer partial and sometimes conflicting assignments of the observed bands [23–28]. A rather detailed analysis of the IR and Raman bands due to the vibrational modes α-$Zr(HPO_4)_2 \cdot H_2O$ layer was given [26] but the interpretation of the complex H-bonding existing among water molecules and phosphate groups is still an open question. In the case of α-$Zr(HPO_4)_2 \cdot H_2O$ the most controversial point is the assignment of the complex structure of bands present in the OH-stretching region generally discussed by considering mainly the vibrations of the water molecule but devoting little attention to the PO–H modes.

More precisely, α-$Zr(HPO_4)_2 \cdot H_2O$ presents two rather sharp peaks at 3593 and 3510 cm^{-1} and a broader band centered around 3150 cm^{-1}, superimposed to a very broad absorption developing from 3400 to 2800 cm^{-1}, unambiguously assignable to OH groups associated as donor or as both donor and acceptor. On the contrary, both shape and separation of the first two peaks would suggest their assignment to OH-stretching bands of water molecules engaged only as an acceptor in H-bondings.

Nevertheless, these bands have been assigned to the (P)O–H stretching vibrations by Trchova et al. [28] in a study of host–guest interactions in α-$Zr(HPO_4)_2$ intercalated by water and ethanol groups, in spite of the strong H-bonding of the (P)O–H groups to the hosted molecules. Previously, a very simple interpretation of the complex features in the OH-stretching region invoked the presence of three different types of interlayer water [27], despite that it disagreed with the observation of Horsely et al. [24] that during dehydration the band intensities decrease with a constant rate. Therefore, these latter authors assumed the presence of equivalent interlayer water molecules and proposed an assignment derived by the symmetry prediction for the presence of four water molecules in the unit cell, which implied the accidental degeneracy of many different modes. This approach, very useful to explain the band splitting of molecular crystals, in our opinion cannot be applied when the H-bonding strongly modifies the electronic structure and the molecular symmetry. In the case of α-$Zr(HPO_4)_2 \cdot H_2O$, in fact, a neutron scattering-based study [21] indicated a rather complicated geometry due to the presence of two non-equivalent POH groups bridged to the lone pair of a water molecule, having one of the two H atoms free and the other bonded to the oxygen atom of a POH group. These data contrast the results of the molecular mechanics simulation of Trchova et al. [28] invoking the presence of a weak interlayer H-bonding. From the spectroscopic point of view, a very interesting result is given by the spectral changes observed after D_2O exchange by both Colomban and Novak [26] and a more detailed study performed at the University of Perugia [29], showing that the position of the two sharp peaks changes by isotopic dilution.

Moreover, no vibrational spectroscopic investigations have been made in order to understand the H-bonding structure of the anhydrous form α-$Zr(HPO_4)_2$ and the very interesting structural modifications following the dehydration process of α-$Zr(HPO_4)_2 \cdot H_2O$ [30,31]. In particular, the layer spacing d shortens from 756 pm in the hydrated crystal to 740 pm in α-$Zr(HPO_4)_2$ and to 680 pm above 500 K with the formation of the new β-$Zr(HPO_4)_2$ phase.

In this frame, we made new spectroscopic investigations to analyze the spectral changes induced on α-$Zr(HPO_4)_2 \cdot H_2O$ and α-$Zr(HPO_4)_2$ by both temperature and isotopic exchange, profiting also by FTIR-PAS, which unlike other FTIR sampling techniques, does not require sample manipulations. However, as the photoacoustic signal depends on both optical and thermal properties of the sample [32,33], the PA spectrum is characteristic of a variable part of the sample beneath the surface and shows bandshapes strictly related to the sample morphology. Therefore, as previously discussed in a detailed study concerning membranes and porous materials [34], affordable results by FTIR-PAS cannot set aside a check of the sample morphology. To this end, several high-purity grade α-$Zr(HPO_4)_2 \cdot H_2O$ and α-$Zr(HPO_4)_2$ of different morphologies have been prepared and characterized by SEM, RX, DSC, TGA and Raman spectroscopy.

2. Experimental

2.1. Preparation of crystalline α-$Zr(HPO_4)_2 \cdot H_2O$

Microcrystalline monohydrated α-zirconium phosphate (hereafter α-$Zr(HPO_4)_2 \cdot H_2O$(cr), crystal size on the micrometer scale) and macrocrystalline monohydrated α-zirconium phosphate (hereafter α-$Zr(HPO_4)_2 \cdot H_2O$(mc), crystal size on the millimeter scale) were prepared by the direct precipitation method in the presence of hydrofluoric acid according to Refs. [35,36], respectively. Microcrystalline anhydrous α-zirconium phosphate (hereafter α-$Zr(HPO_4)_2$(cr)) was obtained by heating the monohydrated material at 130 and 180 °C for 3 days and 6 h, respectively.

2.2. Preparation of amorphous $Zr(HPO_4)_2 \cdot 2.7H_2O$

An aqueous solution of 0.5 M $ZrOCl_2 \cdot 8H_2O$ and 4 M HCl was added drop by drop to a solution of 2 M H_3PO_4 so that the P/Zr molar ratio was 11. The precipitate thus obtained was left at rest for 2 days and washed four times with 0.4 M H_3PO_4 (about 10 mL washing solution/g of solid) and three times with water. The amorphous precipitate was dried in air and stored at 53% relative humidity. The water content, determined by the weight loss at 200 °C, turned out to be 2.7 water molecules/Zr atom. This sample will be hereafter represented as $Zr(HPO_4)_2 \cdot 2.7H_2O$(am).

2.3. Preparation of semicrystalline α-$Zr(HPO_4)_2 \cdot H_2O$

A sample of amorphous zirconium phosphate was refluxed in 7 M H_3PO_4 for 60 h. The solid was then washed several times with 0.01 M HCl (until the H_3PO_4 concentration in the washing solution was lower than 3×10^{-4} M), and finally with deionised water. The solid (hereafter α-$Zr(HPO_4)_2 \cdot H_2O$(sc)) was dried in air and stored at 53% relative humidity.

2.4. Isotopic exchange

The proton exchange by deuterium was obtained by repeated 0.5 h washing of the powders with D_2O excess in a glove-bag flushed by a dried air stream (RH < 15%).

2.5. Instrumentations

SEM images were collected by a SEM LEO, STEREOSCAN 440 scanning electron microscope. FT-Raman (1064 cm^{-1} excitation) and FTIR spectra were recorded with 2 cm^{-1} resolution by Bruker RFS100 and IFS66 spectrometers, respectively. In situ IR transmission measurements were made on KBr pellets with a Specac Variotemp heatable cell. A MTEC Photoacoustics mod.200 cell filled with He was used to obtain FTIR-PAS spectra with 4 cm^{-1} resolution, using carbon black as a reference.

3. Results and discussion

3.1. Samples morphology

Fig. 1 shows the X-ray powder patterns of α-$Zr(HPO_4)_2 \cdot H_2O$(cr), α-$Zr(HPO_4)_2 \cdot H_2O$(sc) and $Zr(HPO_4)_2 \cdot 2.7H_2O$(am); while the microcrystalline and semicrystalline samples exhibit the same main reflections with different intensity and resolution, the pattern of the amorphous material does not show any peak. The different degrees of crystallinity are also associated with a different sample morphology (Fig. 2). It is apparent that microcrystalline samples, both in hydrated α-$Zr(HPO_4)_2 \cdot H_2O$(cr) and in anhydrous α-$Zr(HPO_4)_2$(cr), consist of thin platelets with a rather large size distribution from few hundred nm up to several μm. On the contrary, the semicrystalline α-$Zr(HPO_4)_2 \cdot H_2O$(sc) sample is formed by very small and rather homogeneous crystals with a size of 100–200 nm. The $Zr(HPO_4)_2 \cdot 2.7H_2O$(am) sample is instead formed by big aggregates originated by the merging of particles of several micrometer diameters. Finally the α-$Zr(HPO_4)_2 \cdot H_2O$(mc) samples, not shown, consist of macrocrystals sizing 2–3 mm with variable shape and degree of twinning.

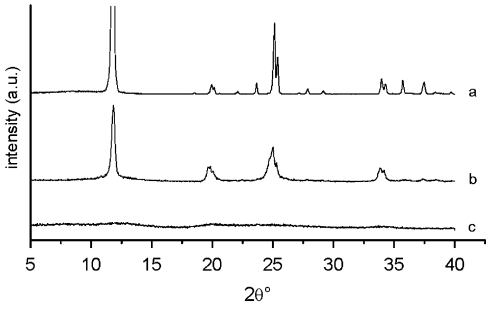

Fig. 1. X-ray powder patterns of (a) α-$Zr(HPO_4)_2 \cdot H_2O$(cr), (b) α-$Zr(HPO_4)_2 \cdot H_2O$(sc) and (c) $Zr(HPO_4)_2 \cdot 2.7H_2O$(am) samples.

3.2. Raman spectra

The study of the OH bands by FT-Raman is practically hindered by the Ge detector limitations for Raman shifts above 3200 cm^{-1} and the very low Raman intensity of the water-bending mode at about 1620 cm^{-1}. Better results have been obtained by micro Raman investigations with visible laser excitations but, as the observed bands strongly depend on the sample orientation, the interpretation of these spectra requires a complete discussion of band polarizations and scattering geometries, which is out of the scope of the present study.

Therefore, at present, only the FT-Raman spectra reported in Fig. 3 are considered. The trace a obtained from α-$Zr(HPO_4)_2 \cdot H_2O$(mc) samples, except for minor differences in the baseline, is practically indistinguishable from the spectra of the other monohydrated samples, clearly indicating that the Raman bands of α-$Zr(HPO_4)_2 \cdot H_2O$ do not depend on the actual sample morphology. By comparison with trace b it is apparent that α-$Zr(HPO_4)_2 \cdot H_2O$ and α-$Zr(HPO_4)_2$ present similar spectra mainly differing for a small shift of several peaks. The main difference is regarding the P–O-stretching region, where by dehydration the modes above 1000 cm^{-1} are about 10 cm^{-1} blushifted while the two bands at 983 and 959 cm^{-1} are replaced by a band at 940 cm^{-1}. It agrees also to the presence of two non-equivalent POH groups in α-$Zr(HPO_4)_2 \cdot H_2O$ [21] and of only equivalent POH groups in α-$Zr(HPO_4)_2$. We propose, in contrast to Ref. [28], their assignment to the stretching of the P–O(H) groups also on the basis of the IR results and isotopic exchange data discussed later on. The two bands at 290 cm^{-1} (strong) and 210 cm^{-1} (weak), involving motions of the Zr and O atoms, show instead a small redshift to 284 and 193 cm^{-1}, respectively.

All these findings seem also to indicate that the layer structure of the two compounds differs only for some electronic redistribution in the phosphate groups. Namely, some loosening of the P–OH bond at expense of a small stiffening of the P–O(Zr) bonds probably occurs in the dehydrated compound.

3.3. FTIR-PAS spectra

The FTIR-PAS spectra of Fig. 4 on the contrary indicate that each sample gives a very different photoacoustic response. The best spectral quality is observed in the case of the α-$Zr(HPO_4)_2 \cdot H_2O$(sc) sample (trace a), which shows

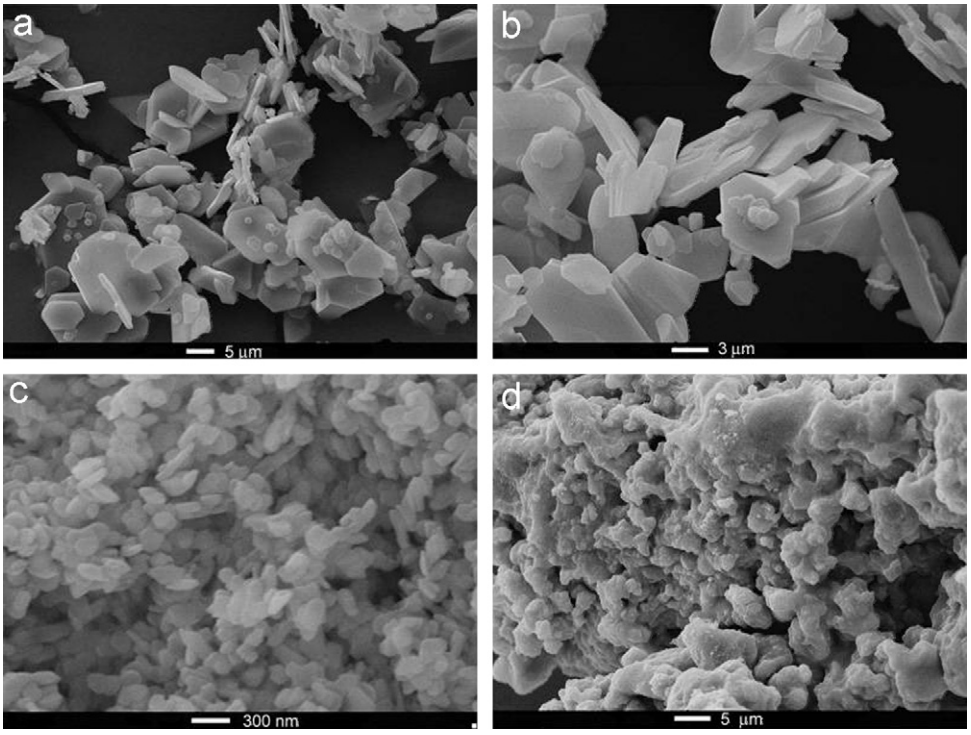

Fig. 2. SEM micrographs of: (a) α-$Zr(HPO_4)_2 \cdot H_2O$(cr), (b) α-$Zr(HPO_4)_2$(cr), (c) α-$Zr(HPO_4)_2 \cdot H_2O$(sc) and (d) $Zr(HPO_4)_2 \cdot 2.7H_2O$(am) samples.

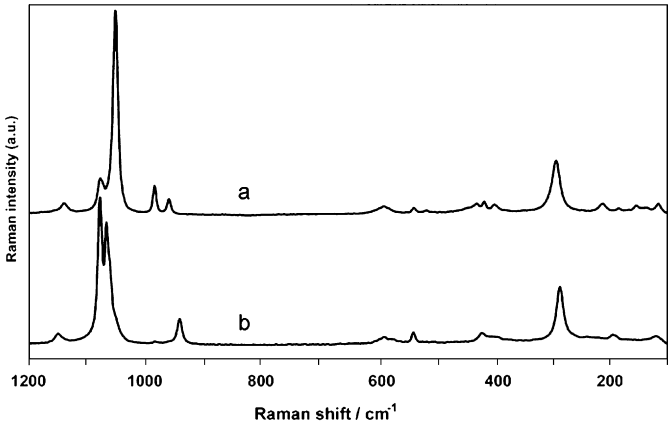

Fig. 3. FT-Raman spectra of: (a) α-$Zr(HPO_4)_2 \cdot H_2O$(mc) and (b) α-$Zr(HPO_4)_2$.(cr) samples.

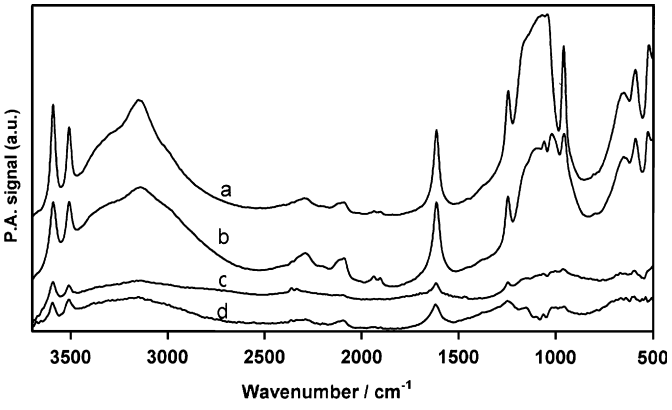

Fig. 4. FTIR-PAS spectra of powders of (a) α-$Zr(HPO_4)_2 \cdot H_2O$(sc), (b) α-$Zr(HPO_4)_2 \cdot H_2O$(cr), (c) $Zr(HPO_4)_2 \cdot 2.7H_2O$(am) samples and (d) of a α-$Zr(HPO_4)_2 \cdot H_2O$(mc) macrocrystal.

well resolved and contrasted peaks. A poor photoacoustic response is instead given by both α-$Zr(HPO_4)_2 \cdot H_2O$(mc) and $Zr(HPO_4)_2 \cdot 2.7H_2O$(am) samples, as shown by trace d and c of Fig. 4, respectively. An intermediate case is given by the PAS spectrum of the α-$Zr(HPO_4)_2 \cdot H_2O$(cr) sample (trace b) showing a poorer contrast and some band broadenings with respect to the α-$Zr(HPO_4)_2 \cdot H_2O$(sc) sample.

These findings can be generally explained by considering the ratio between the thermal diffusion length (μ_s) of the material and the actual particle size of the sample [33,34]. In fact, as the sample thickness becomes larger than μ_s the strongest bands tend to saturate while the weak ones enhance their relative intensity. By taking also into account that an increase of the particle size lowers the useful surface for the heat exchange with the probe gas (He), the relation between the photoacoustic response of each sample in Fig. 4 and its morphology (Fig. 2) can be achieved straightaway.

Nevertheless, two important points must be stressed by considering the PAS spectra in Fig. 4.

The first one is regarding the different shapes observed for the OH-stretching bands of the α-$Zr(HPO_4)_2 \cdot H_2O$ samples below 3400 cm^{-1} which cannot be attributed only to the experimental conditions. In fact, the spectra of α-$Zr(HPO_4)_2 \cdot H_2O$(cr) and α-$Zr(HPO_4)_2 \cdot H_2O$(sc) samples show bands of different width, suggesting the presence of a different distribution of H-bonding strengths in the

two cases. The larger band width in the α-$Zr(HPO_4)_2 \cdot H_2O$(cr) spectrum could reflect the noticeable spread of crystals size with respect to the high dimensional homogeneity of the α-$Zr(HPO_4)_2 \cdot H_2O$(sc) particles. Moreover, the appreciable shift to lower frequency is very likely assignable to the contribution of the larger crystals where the H-bonding can be reinforced by cooperative effects.

Finally, the continuous-like shape of the $Zr(HPO_4)_2 \cdot 2.7H_2O$(am) spectrum below 3000 cm^{-1} can be associated to the presence of layers or clusters of protonated water adsorbed on the strongly irregular surface of this sample [37].

The second very remarkable point in Fig. 4 is the very strong difference that may be found for each sample in the 1200–950 cm^{-1} region where the P–O-stretching bands are expected.

The more complex structure is given by the PAS spectrum of the α-$Zr(HPO_4)_2 \cdot H_2O$(mc) sample where several relative minima are observed from 1200 to 1000 cm^{-1}. The explanation of these findings can be found by considering that, due to the very strong absorption index k of these vibrational modes, the samples strongly reflect the radiation around the resonance frequency. More precisely in the case of particles with large and regular surfaces, like the α-$Zr(HPO_4)_2 \cdot H_2O$(mc) crystals, the Fresnel reflection becomes the dominating effect and only a very thin layer of the sample absorbs photons of the given frequency. Therefore, the amount of heat exchanged between radiation and crystal drops off thereby weakening the photoacoustic signal and a hole in the band may be observed corresponding to the maximum k value.

On the contrary, in the case of the α-$Zr(HPO_4)_2 \cdot H_2O$(sc) sample the reflection plays a minor role as the particles are smaller than the wavelength of the incident radiation. Therefore, the P–O-stretching bands are little affected by the dispersion of the refractive index n and have a shape very similar to that of the absorption index k. This fact, together with the high photoacoustic efficiency derived by the high specific surface area, explains the very good spectral quality of the PAS spectrum in Fig. 4 (trace a) where the strongest band is peaked between 1080 and 1050 cm^{-1}, corresponding to the very strong P–O-stretching modes.

In the case of the α-$Zr(HPO_4)_2 \cdot H_2O$(cr) sample, consisting of crystalline platelets of very different sizes ranging from 300 nm to 20 μm, these bands (Fig. 4, trace b) are the resultant of the photoacoustic response of each particle and have a shape in-between those observed in the spectra of the α-$Zr(HPO_4)_2 \cdot H_2O$(mc) and α-$Zr(HPO_4)_2 \cdot H_2O$(sc) samples.

All these findings must be taken into account as a general problem when FTIR-PAS spectroscopy is applied to investigate ionic crystals and oxides, which often present very strong absorption and very high reflectivity at the frequency of some normal modes of vibration. For instance, a simple examination of the PAS spectrum of the α-$Zr(HPO_4)_2 \cdot H_2O$(cr) sample (Fig. 4 trace b) would suggest the assignment to P–O-stretching modes of two peaks at 1062 and 1024 cm^{-1}, which are instead experimental artifacts depending on the sample morphology.

3.4. α-$Zr(HPO_4)_2 \cdot H_2O$(sc) sample

As the above discussion indicates that the α-$Zr(HPO_4)_2 \cdot H_2O$(sc) sample is the best material to investigate the H-bonding structure by FTIR PAS, the TGA and DSC results indicate that it is also particularly suitable to study the dehydration process α-$Zr(HPO_4)_2 \cdot H_2O \rightarrow$ α-$Zr(HPO_4)_2$.

In fact the TGA results in Fig. 5 indicate that the intercalated water loss above 130 °C is about 6%, a value practically coincident to the stoichiometric expectation, and the DSC thermograms in Fig. 6 show that the endothermic peak around this temperature is present in the first heating cycle (Fig. 6a) and absent in the second heating cycle (Fig. 6b).

Moreover, both curves in Fig. 6 clearly show an endothermic peak above 200 °C during heating and an exothermic peak below this temperature during cooling due to the α-$Zr(HPO_4)_2 \leftrightarrow \beta$-$Zr(HPO_4)_2$ phase transition [38] of the anhydrous compound. This latter material is stable up to 400 °C as only above this temperature a weight loss is observed (Fig. 5), corresponding to the release of a water molecule with formation of the layered zirconium pyrophosphate [38].

The FTIR-PAS spectra in Fig. 7 refer to the α-$Zr(HPO_4)_2 \cdot H_2O$(sc) sample before and after the thermal treatment up to 200 °C and indicate that the dehydration of α-$Zr(HPO_4)_2 \cdot H_2O$ causes the following main changes:

- The complex ν_{OH} band structure present between 3650 and 2800 cm^{-1} collapses in an asymmetric broad band with maximum on the low-frequency side at 3295 cm^{-1},

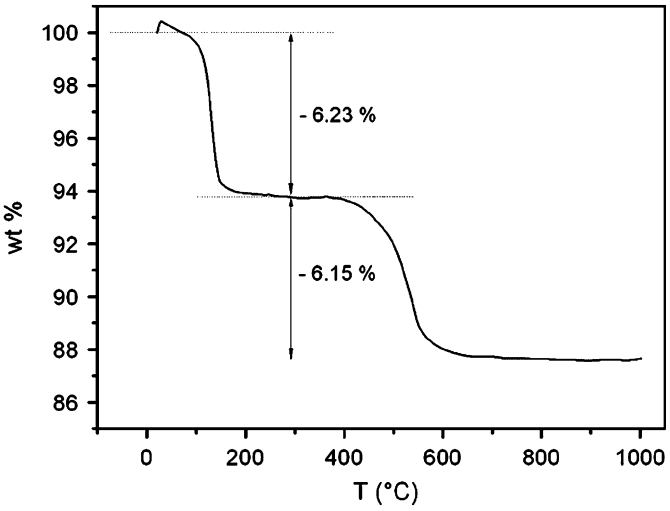

Fig. 5. TGA of the α-$Zr(HPO_4)_2 \cdot H_2O$(sc) sample. Rate of heating: 5 °C/min.

showing that in α-$Zr(HPO_4)_2$ all the POH groups are engaged in H-bonding.

- The 1249 cm^{-1} band moves towards 1200 cm^{-1} merging into the very strong P–O-stretching bands, but its assignment is not straightforward and will be discussed later.
- Unlike the Raman, the IR spectrum shows only one ν_{PO}-stretching band of the P–OH group but a similar shift (30–40 cm^{-1}) is observed after dehydration, confirming both the assignment and the occurrence of some strength redistribution among the P–O bonds as already stated by discussing the Raman spectra.
- The broad band at 654 cm^{-1} vanishes after the water loss, suggesting its assignment to the γ_{OH} torsional mode of the POH groups bonded to water molecules. The assignment of this mode to the bands, observed between 1000 and 950 cm^{-1}, proposed in Ref. [28], seems not reasonable on the basis of three observations: (i) the high frequency, (ii) the bandshape and (iii) its change with temperature.
- Practically no changes are instead observed in both IR and FT-Raman spectra between 600 and 500 cm^{-1}, where the deformation bands of the phosphate groups are expected. The last two spectra were reversibly reproduced during several heating-cooling cycles.
- Between 2500 and 1700 cm^{-1}, several weak or very weak peaks were observed more or less shifted in both α-$Zr(HPO_4)_2 \cdot H_2O$ and α-$Zr(HPO_4)_2$ spectra and, hence, can be assigned to overtone or combination of H-bonding-sensitive fundamental vibrations.

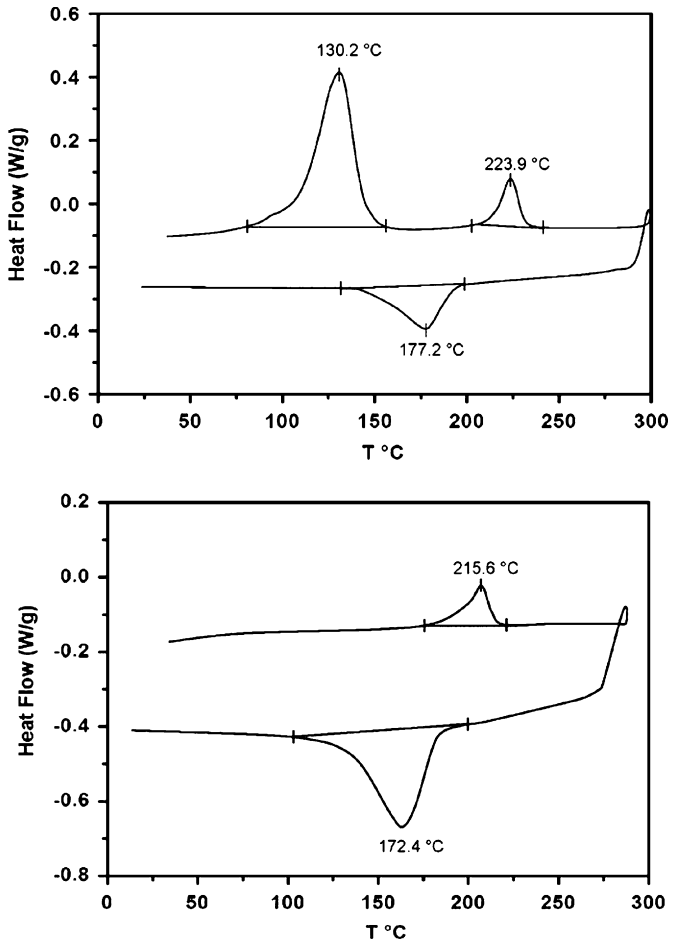

Fig. 6. DSC thermograms for α-$Zr(HPO_4)_2 \cdot H_2O$(sc). Above: first heating cycle. Below: second heating cycle.

The FTIR spectra observed by in-situ transmission measurements (Fig. 7 right) during heating–cooling cycles of the α-$Zr(HPO_4)_2 \cdot H_2O$(sc) sample up to 250 °C clearly indicate that the α-$Zr(HPO_4)_2 \leftrightarrow \beta$-$Zr(HPO_4)_2$ phase transition is accompanied by the change of the H-bonding structure among the POH present on the surface of adjacent layers. In fact, by analyzing the spectra in Fig. 7 it is apparent that at $T = 250$ °C the absorption maximum of the ν_{OH} band is observed at about 3540 cm^{-1} corresponding to the high-frequency side of the band.

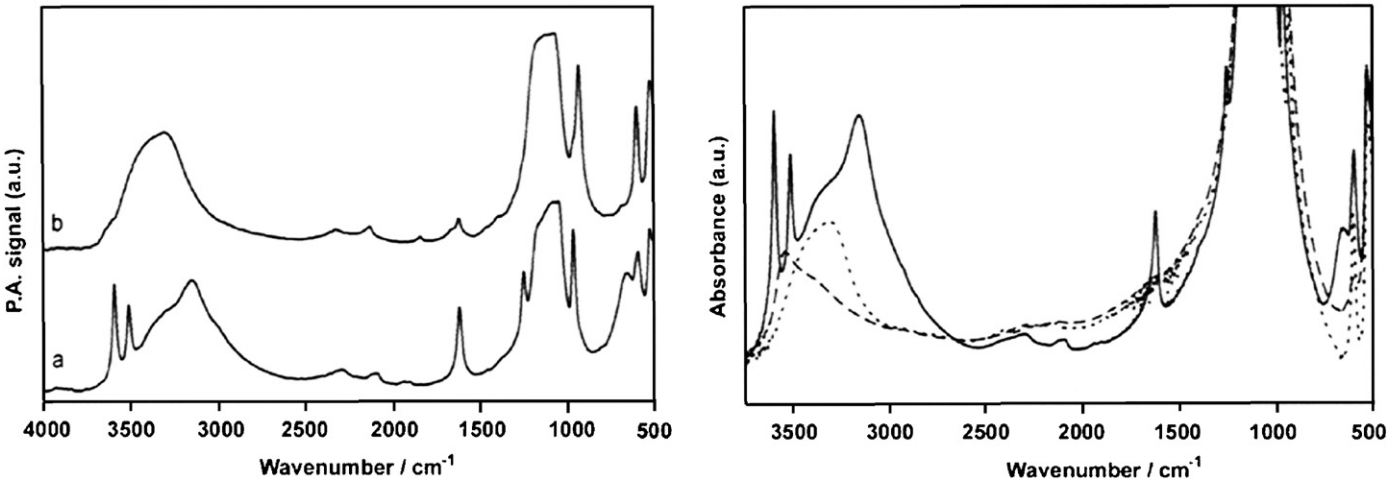

Fig. 7. FTIR spectra of the α-$Zr(HPO_4)_2 \cdot H_2O$(sc) sample. Left: PAS spectra (a) before and (b) after a thermal treatment up to 200 °C. Right: transmission spectra (KBr pellet) observed in-situ during a thermal treatment at: (full line) 25 °C before heating, (dotted line) 25 °C after cooling and (broken line) 250 °C. The last two spectra were reversibly reproduced during several heating-cooling cycles.

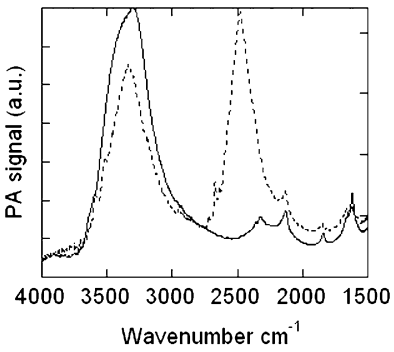

Fig. 8. FTIR-PAS spectra of anhydrous α-$Zr(HPO_4)_2$(sc) in the O–H and O–D-stretching regions: (full line) pristine sample, (dotted line) after a 0.5 h D_2O treatment.

Moreover, during the cooling an isosbestic point is observed, and the temperature range where the switching of the bandshape occurs agrees with the change of phase as shown in Fig. 5. The same features and isosbestic points were observed during several heating-cooling cycles according to the presence of a reversible process like a phase transition.

A deeper insight into the origin of the observed ν_{OH} band is finally given by the results of treatments of α-$Zr(HPO_4)_2$ by D_2O as shown in Fig. 8.

It is known that anhydrous crystalline α-$Zr(HPO_4)_2$ is not able to rehydrate even if dipped in boiling water [39]. On the other hand, α-zirconium phosphate conducts protons even in anhydrous form [40]. Therefore, the treatment of α-$Zr(HPO_4)_2$ by D_2O should result in the exchange of deuterium ions for protons, while leaving α-$Zr(DPO_4)_2$ anhydrous. Fig. 8 shows the comparison of the spectra observed in the OH/OD-stretching region before and after a 0.5 h treatment at 25 °C of an α-$Zr(HPO_4)_2$(sc) sample. The partial isotopic exchange originates a symmetric ν_{PO-D} band with maximum around 2480 cm^{-1} accompanied by a change of shape of the ν_{PO-H} band that becomes almost symmetric with the center at 3340 cm^{-1}. The shape of the ν_{PO-H} and ν_{PO-D} bands in Fig. 8 are similar, except for the smaller width of the latter band due to the notably lower anharmonicity of the OD-stretching mode with respect the OH one. As expected, no bands assignable to H_2O, D_2O or HOD are detected.

These findings strictly reproduce what is generally observed by isotopic dilution in the IR spectra of alcohols and phenols forming polymeric chains of H-bonded OH groups in the solid state [41]. In such polymeric associations, the O–H oscillators are mechanically coupled and, depending on the type of repeating unit, originate two or more ν_{OH} bands shifted with respect to the uncoupled oscillator frequency. Generally these bands can be resolved only at low temperature or by polarized light measurements on monocrystals or oriented samples [42,43], while only an unresolved broader band is observed in the conventional spectrum.

However, as the mechanical coupling vanishes by isotopic dilution, the bands observed in the α-$Zr(HPO_4)_2$ spectrum (Fig. 8, dotted line) have absorption maximum at the frequencies of the uncoupled OH(D)-stretching bands, and the ratio ν_{OH}/ν_{OD} found ($\approx$1.347) is slightly higher than in the case of alcohols and phenols, indicating the presence of a medium-weak H-bond. A distance of about 284 pm between the two bonded oxygen atoms may be assumed on the basis of the ν_{OH} vs. R_{OO} correlations [42–44]. At present, no monocrystal suitable for FTIR investigation by polarized light could be obtained in order to resolve the ν_{OH} band of the protonated material (Fig. 8, full line) but, similarly to what is observed for the H-bonds chain of alcohols and phenols, its shape can be reasonably considered the envelope of two components splitted by a little less than 100 cm^{-1} at both sides of the uncoupled mode frequency.

This interpretation is also consistent with the spectroscopic observation at high temperature. In fact, both strength and lifetime of the H-bonds decrease by heating causing a shortening of the chain length and the enhancement of the number of terminal OH groups. Half of these latter, being bonded only as acceptors, absorb about 200 cm^{-1} above the frequency of the skeletal OH groups, which are also bonded as donors. The other half of OH terminals, being bonded only as donors, absorb at a frequency slightly higher than the skeletal ones. Therefore, the shape of the asymmetric ν_{OH} band reflects the actual distribution of chain lengths in the material: long polymers show a band with maximum at the lower frequency side while the opposite form is observed for dimers and short oligomers.

By taking into account these facts, the changes observed for the ν_{OH} bands in Fig. 7 also suggest that the length of the OH chains must be related to the α-$Zr(HPO_4)_2 \leftrightarrow$ β-$Zr(HPO_4)_2$ phase transition, which, as indicated by a crystallographic study [31], implies a shortening of the layer spacing as well as a change of the crystal symmetry from monoclinic to hexagonal. In this picture it seems reasonable to think that the length of the O–[–H…O–]$_n$–H polymers below a critical mean value ($\langle n_c \rangle$) cannot provide the cooperative strengthening necessary to stabilize the small tilt of the planes present in the monoclinic form [20]. As the temperature exceeds the corresponding critical value, all the OH groups are H-bonded in small aggregates or simply in pairs allowing the planes to relax in the more symmetric hexagonal crystal, where each PO–H group can form the H-bond following three equivalent ways.

As said at the beginning, the α-$Zr(HPO_4)_2 \cdot H_2O$ IR spectrum presents a complex absorption from 3600 to 2900 cm^{-1} due to superposition of the O–H-stretching of water and PO–H groups associated through H-bonds of various strengths but not yet unambiguously assigned. A very significant help to solve this problem is offered by the analysis of the spectral changes observed for the α-$Zr(HPO_4)_2 \cdot H_2O$(sc) sample at different degrees of isotopic exchange resulting after repeated D_2O washing and shown in Fig. 9. It is apparent that as the H/D exchange progresses, the ν_{OH}-stretching bands are replaced by very similar bands developing from 2700 to 2100 cm^{-1}

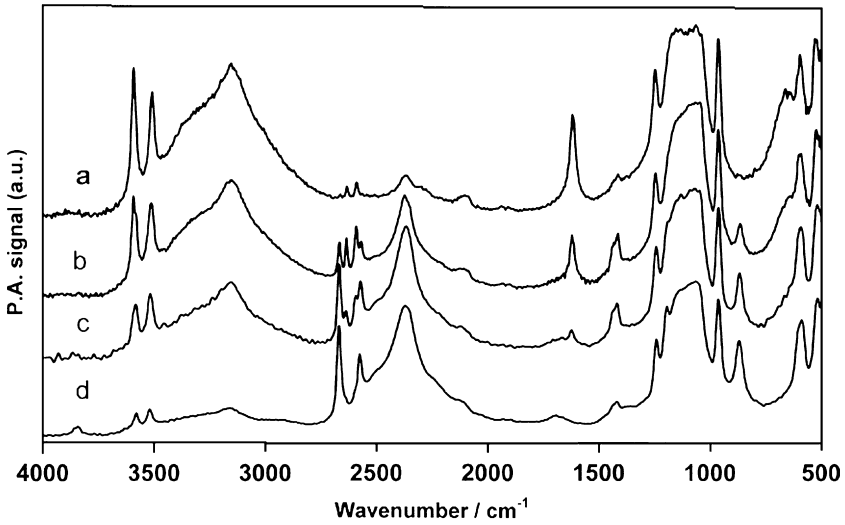

Fig. 9. FTIR-PAS spectra of α-$Zr(HPO_4)_2 \cdot H_2O$(sc) powders at different isotopic exchange, observed after nD_2O treatments: (a) $n = 1$, (b) $n = 2$, (c) $n = 3$ and (d) $n = 5$.

Table 1
Observed α-$Zr(HPO_4)_2 \cdot H_2O$ bands in the O–H(D) stretching region

Stretching vibration	OH/cm^{-1}	OD/cm^{-1}	Isotopic ratio
Band I	3592	2667	1.347
Band I uncoupled	3580	2634	1.359
Band II uncoupled	3516	2590	1.357
Band II	3510	2571	1.365
Band III	3400–2850	2500–2100	$\approx$1.36
Band IV	3152	2366	1.332

except for the smaller width due to the lower anharmonicity of the O–D-stretching vibration. By considering both shape and isotopic ν_{OH}/ν_{OD} ratio, four components I, II, III and IV, as indicated in Table 1, can be distinguished.

The first two components consist of fairly narrow peaks, suggestive of vibrations of OH groups bonded only as acceptors, which change appreciably on the degrees of isotopic exchange. All the experimental evidences are consistent with the presence of two ν_{OH} modes of distinct water molecules weakly coupled by the crystalline field in the elemental cell. As the width of the ν_{OH} peaks does not allow their resolution, the uncoupled peak can be observed only at high degree of isotopic exchange. On the contrary, being sharper for the lower anharmonicity, the ν_{OD} peaks can be resolved as doublets with variable relative intensity. The isotopic ν_{OH}/ν_{OD} ratios in Table 1 clearly indicate that the uncoupled modes, unlike those of the coupled ones, agree very well with the expected value for the considered type of H-bonding.

Other experimental results confirm however the above assignments: (i) except for the bandwidth, an absolute correspondence of the OH/OD bands is observed for all the isotopic exchange degrees; (ii) the Raman polarization data indicate that the bands of the coupled modes belong to different symmetry species, as expected for in-phase and out of phase vibrations of two oscillators in the crystalline unit; (iii) the coupled and uncoupled peaks have opposite relative intensities (Fig. 9) according to the fact that both value and orientation of the dipole moments must be very different for coupled or uncoupled modes.

With regard to the other two components indicated as band III and band IV in Table 1, it must be observed that both position and width are consistent with OH vibrations of groups bonded as donors. The band III is very broad and could derive from the merging of the stretching bands of the second OH group of the water molecule in the unit cell, which, according to the structure determinations [20,21], would be bonded to the oxygen atom of a POH group. These bands, as it occurs for the I and II bands, are very probably slightly splitted but, being intrinsically broad, originate the very large unresolved band III. Finally, the stronger and better defined band IV of Table 1 could be assigned to the stretching of the PO–H groups, which are present in the ratio 2:1 with respect the HO–H donors. This assignment, as discussed before, is compatible also with the results of the dehydration studies but implies that the frequencies of the two non-equivalent POH groups differ for less than the observed half-bandwidth, i.e. about 180 and 100 cm^{-1} for ν_{PO-H} and ν_{PO-D}, respectively. These values can be considered reasonable in the case of spectra obtained at room temperature but a final settlement of this matter cannot be made without the analysis of the vibrational spectra acquired at low temperature and, possibly, on oriented crystals.

The discussion of the other vibrational bands sensitive to the isotopic exchange is simpler and can be summarized as follows:

- The OH-bending δ_{HOH} gives a fairly sharp strong band at 1618 cm^{-1} in the IR spectrum. In the Raman spectrum it is very weak and can be observed only for particular orientations of the α-$Zr(HPO_4)_2 \cdot H_2O$(mc) macrocrystals by microRaman. The corresponding

δ_{DOD} band can be assigned to the peak observed at about 1190 cm^{-1} in the FTIR spectrum of the sample with the highest isotopic exchange degree, overlapped to the very strong P–O-stretching bands. The isotopic ratio $\delta_{OH}/\delta_{OD} \approx 1.37$ seems to confirm to this assignment.

- The δ_{HOD}-bending band of the HOD molecules is observed around 1420 cm^{-1} with maximum intensity at the intermediate degree of isotopic exchange with a shoulder at about 1438 cm^{-1}. As the bending frequency of HOD bonded to D_2O [45] is 1450 cm^{-1}, the doublet is probably related to the two possible states of the molecule, i.e. D or H atom bonded.
- The new band growing up at 868 cm^{-1} can be unambiguously assigned to the δ_{POD}-bending vibrations of the P–O–D group. The corresponding δ_{POH} vibration, on the basis of the expected isotopic shift, would be observed in the range 1230–1180 cm^{-1}, where the isotopic exchange induces two modifications: one is the redshifting and weakening of the 1249 cm^{-1} band; the other is a sensible depletion around 1180 cm^{-1} of the very strong 1200-1000 cm^{-1} structured band. As a weak band at 1238 cm^{-1} is present also in the case of α-$Zr(DPO_4)_2 \cdot D_2O$ [29], these results seem to indicate that in the case of α-$Zr(HPO_4)_2 \cdot H_2O$, due to accidental degeneracy, some mechanical coupling among a P–O-stretching mode and the δ_{POH} occurs.
- The assignment of the fairly broad band at 654 cm^{-1} to the γ_{OH} torsional mode of the POH groups bonded to water molecules is confirmed by its rapid depleting as the isotopic exchange proceeds. In fact, as expected by the isotopic effect, a new absorption on the low-frequency side of the strong 530 cm^{-1} band γ_{OD} is observed at about 490 cm^{-1}.

3.5. α-$Zr(HPO_4)_2 \cdot H_2O$(cr) and α-$Zr(HPO_4)_2$(cr) samples

The FTIR spectra of Fig. 10 observed during the thermal treatments of the α-$Zr(HPO_4)_2 \cdot H_2O$(cr) sample, otherwise the α-$Zr(HPO_4)_2 \cdot H_2O$(sc) corresponding spectrum (Fig. 7), shows that above 200 °C a water O–H-stretching band around 3615 cm^{-1} is still present. Moreover, the spectra observed after repeated or long heating, in addition to those of the α-$Zr(HPO_4)_2$, retain an appreciable amount of the characteristic bands of α-$Zr(HPO_4)_2 \cdot H_2O$ and show an appreciable blue shift of the band IV.

The effects of the isotopic exchange in the spectrum are identical to those discussed above for the α-$Zr(HPO_4)_2 \cdot H_2O$(sc) sample but the exchange rate is very low also at high temperature.

All these findings clearly indicate that, according to Ref. [46], the water molecules run into some difficulties to leave the large α-$Zr(HPO_4)_2 \cdot H_2O$(cr) crystals and agree with the presence of appreciable cooperative reinforcing of the H-bonding as the layer surface increases.

The FT-Raman spectra of both α-$Zr(HPO_4)_2$ samples (α-$Zr(HPO_4)_2$(cr) and α-$Zr(HPO_4)_2$ (sc)) are practically indistinguishable. Otherwise, the FTIR-PAS spectra of the α-$Zr(HPO_4)_2$(cr) sample also show fairly intense OH bands characteristic of α-$Zr(HPO_4)_2 \cdot H_2O$ indicating the presence of appreciable amounts of the hydrated form. This fact confirms that both techniques must be used to well characterize such types of materials.

3.6. $Zr(HPO_4)_2 \cdot 2.7H_2O$(am) sample

The PAS spectrum of the $Zr(HPO_4)_2 \cdot 2.7H_2O$(am) sample, shown in Fig. 11 (full line), can be considered as the superposition of a broad continuum-like feature, developing below 3500 cm^{-1}, to the typical bands of α-$Zr(HPO_4)_2 \cdot H_2O$ already discussed regarding the α-$Zr(HPO_4)_2 \cdot H_2O$(sc) spectrum. By heating above 100 °C, the OH peaks characteristic of the interlayer water disappear but the continuum like spectral features are still present. These continuum-like O–H bands are characteristic of easily polarizable H-bonds and are generally observed in the case-protonated water clusters [37]. Further heating above 180 °C causes several changes of the low-frequency bands characteristic of the α-zirconium phosphate layer structure. Unfortunately, the Raman spectrum

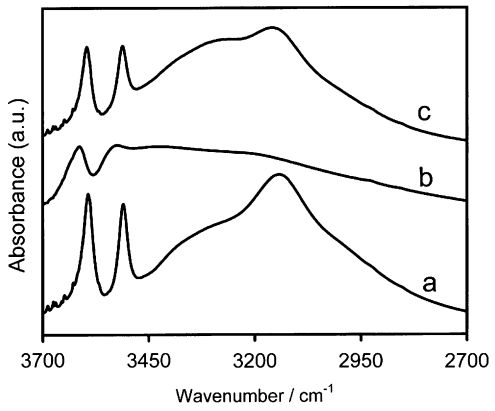

Fig. 10. FTIR transmission spectra (KBr pellet) observed in-situ during a thermal treatment of the α-$Zr(HPO_4)_2 \cdot H_2O$(cr) sample: (a) 25 °C before heating, (b) 200 °C and (c) 25 °C after cooling.

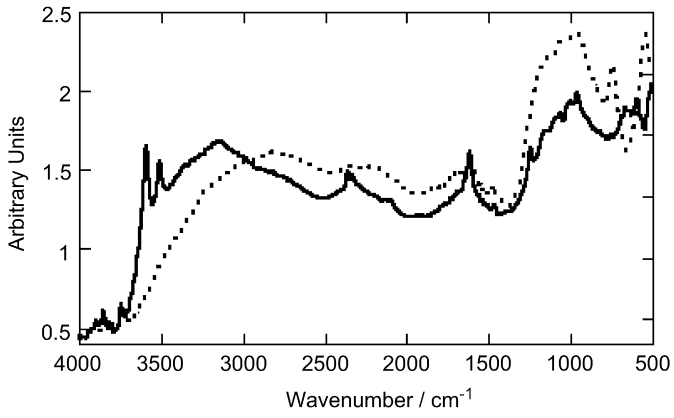

Fig. 11. FTIR-PAS spectra of the $Zr(HPO_4)_2 \cdot 2.7H_2O$(am) sample: (full line) pristine sample, (dotted line) after heating above 180 °C.

is strongly affected by luminescence and only a small peak at about 1085 cm^{-1} can be appreciated. All these facts suggest that the amorphous $Zr(HPO_4)_2 \cdot 2.7H_2O$(am) sample mainly contains very disordered structures of phosphate units and bonded water formed on the surface of small crystals of α-$Zr(HPO_4)_2 \cdot H_2O$. The latter easily loose the interlayer water molecules by heating but the process causes a marked structural change of the dominant disordered material, which, due to its high specific area and the acidity of the surface POH groups, strongly absorb water clusters. However the contribution of the latter in the spectra in Fig. 11 can be highly overestimated with respect to the bulk of the sample by taking into account both the high absorption coefficient of water cluster and the surface sensitivity of the PAS technique. Nevertheless, the occurrence of remarkable structural changes is confirmed by the DSC results, which markedly differ from those of α-$Zr(HPO_4)_2 \cdot H_2O$(sc) and α-$Zr(HPO_4)_2 \cdot H_2O$(cr) samples, discussed above, showing an irreversible transformation after the first heating up to 250 °C.

For all these reasons, a deeper insight into this matter requires new data, possibly obtained by complementary techniques to the vibrational ones.

4. Conclusions

The analysis of IR and Raman spectra clearly shows that there is a close relation between the morphology of the sample and the order existing between the layers of Zr phosphate.

The FT-Raman spectra are useful mainly for the characterization of the Zr phosphate layer structure being poorly sensitive to H-bondings of both PO–H groups and water molecules. In spite of the very different morphology, all the samples presented the characteristic Raman spectrum of the crystalline Zr phosphate layer, also in the case of samples classified as semicrystalline or amorphous by the X-ray analysis. Due to the breakdown of the selection rules, changes of both band width and position can be observed only in the case of nanometric particles like those obtained from gels of exfoliated Zr phosphates. The analysis of such types of samples is in progress.

The FTIR spectra are a key tool to detect the presence of water molecules as well as to investigate the H-bonds structure of the different forms. Very different structures of the interlayer water can be observed as a function of the sample morphology. In particular, the FTIR analysis allows understanding the structural changes involved in phase transitions, proton exchange and hydration–dehydration processes. Several restrictions for the study of the layer structure are instead put by the very strong absorption of the P–O-stretching band.

The water molecule in the α-$Zr(HPO_4)_2 \cdot H_2O$ crystal presents very characteristic infrared bands in both the OH-stretching and bending region that, in agreement with Ref. [21], can be assigned to a very regular hydrogen bonding of each molecule to three adjacent OH groups (two donors and one acceptor) belonging to the same layer side. Nevertheless, in contrast to Refs. [21,31], the four water molecules present in the unit cell cannot be considered equivalent from the vibrational point of view, indicating the presence of two types of water molecules. This fact can be reasonably explained by taking into account that, within the errors of the structural determination, the position of the water H atoms may be different from that expected for crystallographically equivalent water molecules, thus leading to the breakdown of the symmetry. Moreover, the particular H-bonding structure slightly couples the stretching vibration of the free H atom of the two water molecules in the unit cell.

Amorphous samples also develop a more or less intense continuum-like spectrum characteristic of some protonated water cluster or film adsorbed on the high sample surface.

The POH groups in the anhydrous α-$Zr(HPO_4)_2$ crystal, similar to many alcohols, form OH chains along which the proton can switch. By heating, due to the lower lifetime of the H-bonds, the polymeric OH structure shortens allowing the formation of the β-$Zr(HPO_4)_2$ phase where the POH groups are bonded mainly in pairs. The cooperative strengthening of H-bonds fades as the chains shorten, allowing an appreciable release of both the intra- and interlayer structure.

At low temperature the anhydrous α-$Zr(HPO_4)_2$ crystal however cannot be easily hydrated but a quite rapid H/D exchange in the POH groups occurs in D_2O. This fact agrees with the existence of a protonic conduction mechanism occurring through the above-discussed H-bonds chains. On the contrary this type of H-bonding determines an unfavorable interlayer geometry and stability hindering the water molecule to enter. It must however be stressed that the presence of cooperative effects in the H-bonding mechanisms as well as the van der Waals dispersion forces between adjacent layers stabilize appreciably the larger crystals of α-$Zr(HPO_4)_2 \cdot H_2O$. In this case, as the diffusion of H_2O or $D+$ occurs along the layers starting from the crystal edge, a slowing down of both dehydration and isotope exchange is observed. Moreover, as the reaction α-$Zr(HPO_4)_2 \cdot H_2O \rightarrow \alpha$-$Zr(HPO_4)_2$ implies the shortening of the interlayer distance, in the case of macrocrystals the water molecules, present in the inner part of the crystal, can remain entrapped between the layers for a long time also at 250 °C.

All these facts indicate that vibrational spectra are very effective in characterizing Zr phosphates, giving also some useful indication about the sample morphology. Finally the proposed band assignments offer a reliable basis to study the different forms and possible modifications in such types of materials.

Acknowledgment

This work was supported by MIUR within the FISR 2001 project "Nanocompositi ibridi a matrice polimerica organica e cariche nanostrutturanti inorganiche".

References

[1] W. Grot, G. Rajendran, Patent No. WO 96/2975, 1996.
[2] P. Costamagna, C. Yang, A.B. Bocarsly, S. Srinivasan, Electrochim. Acta 47 (2002) 1023.
[3] C. Yang, S. Srinivasan, A.S. Aricò, P. Creti, V. Baglio, V. Antonucci, Electrochem. Solid-State Lett. 4 (2001) A31.
[4] C. Yang, S. Srinivasan, A.B. Bocarsly, S. Tulyani, J.B. Benziger, J. Membr. Sci. 237 (2004) 145.
[5] S.K. Tiwari, S.K. Nema, Y.K. Agarwal, Thermochim. Acta 317 (1998) 175.
[6] F. Bauer, M. Willert-Porada, J. Membr. Sci. 233 (2004) 141.
[7] M.K. Song, Y.T. Kim, J.S. Hwang, H.Y. Ha, H.W. Rhee, Electrochem. Solid-State Lett. 7 (2004) A127.
[8] B. Bonnet, D.J. Jones, J. Rozière, L. Tchicaya, G. Alberti, M. Casciola, L. Massinelli, B. Bauer, A. Peraio, E. Ramunni, J. New Mater. Electrochem. Syst. 3 (2000) 87.
[9] D.J. Jones, J. Rozière, J. Membr. Sci. 185 (2001) 41.
[10] L. Tchicaya-Bouckary, D.J. Jones, J. Rozière, Fuel Cells—from Fundamentals to Applications, Vol. 2, Wiley, New York, 2002, p. 40.
[11] S.P. Nunes, B. Ruffmann, E. Rikowski, S. Vetter, K. Richau, J. Membr. Sci. 203 (2002) 215.
[12] L.A.S.De A. Prado, H. Wittich, K. Schulte, G. Goerigk, V.M. Garamus, R. Wilumeit, S. Vetter, B. Ruffmann, S.P. Nunes, J. Polym. Sci. B 42 (2003) 567.
[13] B. Ruffmann, H. Silva, B. Schulte, S.P. Nunes, Solid State Ion. 162–163 (2003) 269.
[14] H.J. Sue, K.T. Gam, N. Bestaoui, N. Spurr, A. Clearfield, Chem. Mater. 16 (2004) 242.
[15] H.J. Sue, K.T. Gam, N. Bestaoui, A. Clearfield, M. Miyamoto, N. Miyatake, Acta Mater. 52 (2004) 2239–2250.
[16] J. Wang, Y. Hu, B. Li, Z. Gui, Z. Chen, Ultrason. Sonochem. 11 (2004) 301.
[17] M. Casciola, G. Alberti, A. Donnadio, M. Pica, A. Bottino, P. Piaggio, J. Mater. Chem. 15 (2005) 4262.
[18] M. Casciola, A. Donnadio, M. Pica, V. Valentini, P. Piaggio, Macromolec. Symp. 230 (2005) 95.
[19] A. Clearfield, G.D. Smith, Inorg. Chem. 8 (1969) 431.
[20] J.M. Troup, A. Clearfield, Inorg. Chem. 16 (1977) 3311.
[21] J. Albertsson, A. Oskarsson, R. Tellgren, J.O. Thomas, J. Phys. Chem. 81 (1977) 1574.
[22] A. Clearfield, S.P. Pack, J. Inorg. Nucl. Chem. 37 (1975) 1283.
[23] R.C.T. Slade, J.A. Knowles, D.J. Jones, J. Roziere, Solid State Ion. 96 (1997) 9.
[24] S.E. Horseley, D.V. Nowell, D.T. Stewart, Spectrochim. Acta 30A (1974) 535.
[25] A. Rulmont, R. Cahay, M. Liegeois-Duyckaerts, P. Tartre, Eur. J. Solid State Inorg. Chem. 28 (1991) 207.
[26] P. Colomban, A.J. Novak, Mol. Struct. 198 (1989) 277.
[27] X. Mathew, V.U. Nayar, Infrared Phys. 3 (1988) 189.
[28] M. Trchova, P. Capkova, P. Matejka, K. Melanoma, L. Benes, J. Solid State Chem. 145 (1999) 1.
[29] G. Fiorio, D. Chem. Thesis, Department of Chemistry, University of Perugia, 1974.
[30] A. La Ginestra, M.A. Massucci, C. Ferragina, N. Tomassini, Thermoanalysis, in: Proceedings of IV ICTA, Budapest 1, 1974, p. 631.
[31] G. Schuck, R. Melzer, R. Sonntag, R.E. Lechner, A. Bohn, K. Langer, M. Casciola, Solid State Ion. 77 (1995) 55.
[32] A. Rosencwaig, A. Gersho, J. Appl. Phys. 47 (1976) 64.
[33] J.M. Chalmers, G. Dent, Industrial Analysis with Vibrational Spectroscopy, The Royal Society of Chemistry, Cambridge, 1997, p. 155.
[34] T. Boccaccio, A. Bottino, G. Capannelli, P. Piaggio, J. Membr. Sci. 210 (2002) 315.
[35] G. Alberti, S. Allulli, U. Costantino, M.A. Massucci, J. Inorg. Nucl. Chem. 37 (1975) 1779.
[36] G. Alberti, U. Costantino, R. Giulietti, J. Inorg. Nucl. Chem. 42 (1980) 1062.
[37] G. Zundel, in: The Hydrogen Bond, vol. II, North-Holland Publishing Company, Amsterdam, 1977, p. 683.
[38] U. Costantino, A. La Ginestra, Thermochim. Acta 58 (1982) 179.
[39] M. Casciola, F. Marmottini, A. Peraio, Solid State Ion. 61 (1993) 125.
[40] G. Alberti, M. Casciola, U. Costantino, R. Radi, Gazz. Chim. Ital. 109 (1979) 421.
[41] R.J. Jakobsen, J.W. Brasch, Y. Mikawa, J. Mol. Struct. 1 (1967–68) 309.
[42] P. Piaggio, M. Rui, R. Tubino, G. Dellepiane, Spectrochim. Acta 8 (1982) 913.
[43] P. Piaggio, R. Tubino, G. Dellepiane, J. Mol. Struct. 96 (1983) 277–281.
[44] D. Hadzi, S. Bratos, in: The Hydrogen Bond, vol. II, North-Holland Publishing Company, Amsterdam, 1977 p. 575.
[45] A.J. Lock, H.J. Bakker, J. Chem. Phys. 117 (2002) 1708–1713.
[46] A. Clearfield, U. Costantino, in: G. Alberti, T. Bein (Eds.), Comprehensive Supramolecular Chemistry, vol. 7, Elsevier Science Ltd Press, Pergamon, 1996 (chapter 4).